A Subharmonic Self-Oscillating Mixer with Integrated Antenna for 60-GHz Wireless Applications

Mikko Sironen, Yongxi Qian, *Member, IEEE,* and Tatsuo Itoh, *Life Member, IEEE*

***Abstract*—A balanced integrated-antenna self-oscillating mixer at 60 GHz is presented in this paper. The modal radiation characteristics of a dual-feed planar quasi-Yagi antenna are used to achieve RF–local oscillator (RF–LO) isolation between closely spaced frequencies. The balanced mixer is symmetric, inherently broad band, and does not need an RF balun. Pseudomorphic high electron-mobility transistors are used in a 30-GHz push–pull circuit to generate the second harmonic and a 30-GHz dielectric resonator was used to stabilize the fundamental oscillation frequency. This allows the possibility of building a balanced low-cost self-contained antenna integrated receiver with low LO leakage for short-range narrow-band communication. Phase locking can be done with half of the RF frequency. The circuit exhibits a conversion loss less than 15 dB from 60 to 61.5 GHz, radiation leakage of −26 dBm at 60 GHz, and IF phase noise of −95 dBc/Hz at 100-kHz offset.**

***Index Terms*—Millimeter wave, planar integrated antenna, self-oscillating mixer, wireless.**

I. Introduction

In THIS paper, a novel integrated-antenna receiver front-end is introduced. The RF frequency is 60 GHz, allowing high data transmission rates. This high-frequency design results in a compact planar design, which is highly desired in many developing commercial applications. One possible application is real-time transmission of digital video signals. The receiver incorporates several novel features. First, the receiver is directly integrated with a planar quasi-Yagi antenna, which provides the basis for a simple balanced design. Next, a second harmonic self-oscillating mixer (SOM) is used, with a number of benefits, including reduced cost through lowered component count, the ability to use devices with a lower $f_{\max}$, and the commercial availability of dielectric resonators (DRs) at 30 GHz.

The broad-band quasi-Yagi antenna, with an endfire beam and a good front-to-back ratio, is fabricated on a high dielectric-constant substrate and demonstrates a good radiation characteristic [1]. A single balanced receiver circuit can be built with this antenna without using an RF balun, allowing a simple and compact design. Antennas nonradiative mode can be used as a reactive circuit element, as will be demonstrated.

Manuscript received September 7, 1999. This work was supported by Sony under RF Front-Ends for 60 GHz Multimedia Wireless System MICRO and by the Army Research Office under the Multidisciplinary Research Initiative on Low Power Electronics.

The authors are with the Department of Electrical Engineering, University of California at Los Angeles, Los Angeles, CA 90095 USA.

Publisher Item Identifier S 0018-9480(01)01678-7.

In a SOM configuration, a single device simultaneously provides both oscillator and mixing functions. Typically, SOMs are operated as a Doppler detector, even in subharmonic mode, because typical Doppler bandwidths are in the kilohertz range and, therefore, a very high noise figure can be tolerated. As demand for wireless data transmission increases, bandwidth requirements for several new communication applications are being pushed in the megahertz range. Since the minimum detectable signal at larger IF frequencies is improved due to the low-frequency noise behavior of the device, a subharmonic SOM without preamplifier becomes a possibility in short-range applications.

Since the introduction of the first FET SOM in [2], variants of SOM operation mode have been demonstrated. A SOM in [3] demonstrated 3-dB conversion gain and 9.5-dB double sideband (DSB) noise figure, with a 9.5-GHz DR used to stabilize the frequency. The first subharmonic SOM [4] was operated at 34 GHz with 5% conversion efficiency and −121.6-dBm/Hz detection sensitivity at 4 kHz. This subharmonic SOM demonstrates that FETs with $f_{\max}$ less than the RF frequency can be used. A fundamentally operated balanced SOM [5] integrated with a slot antenna had 4-dB conversion gain and an 8-dB noise figure. This SOM was operated at zero gate bias and at the knee of the IV curve. A second harmonic monolithic-microwave integrated-circuit (MMIC) SOM [6] at W-band showed 15-dB conversion loss over more than a 15-GHz bandwidth. Wide bandwidth was achieved by using a novel feedback structure. The same SOM was also used for optical demodulation in [7], and conversion gain was achieved for the induced RF power. In [8], a DR stabilized push–pull oscillator was used as a balanced optical up-converter internal local oscillator (LO) was effectively suppressed at the IF port.

RF–LO isolation must be addressed when designing an integrated antenna SOM. In [5] and [8], isolation was achieved by using a balanced layout. In [9], a cavity-backed antenna with a sharp radiation null at the resonance frequency was used. In this case, LO power is dissipated in a resistor specifically placed so that RF reception is not affected, thereby reducing radiation of the LO. Another crucial factor is phase stability, which is often not sufficient when standard microwave resonators are used because of the typically low Q-factor. Coherent detection is possible by using a phase-controlled SOM [10], which has large locking range, low phase noise, and high conversion efficiency. An additional phase reference is required.

The DR balanced second harmonic antenna-integrated SOM at 60 GHz is optimized for 1-GHz IF. A high electron-mobility transistor (HEMT) device with $f_{\max}$ less than the RF frequency

was used in the harmonic generation, and the phase stability requirement is approached by using a high-Q DR in $\mathrm{TE}_{01\delta}$ mode. A balanced push–pull oscillator is used to enhance the generation of the second harmonic; this allows direct integration with a dual-feed antenna to solve the radiation problem. With these choices, the mixer has the potential for use in low-cost components and low LO leakage, while giving useful conversion gain, noise figure, and phase stability. In this paper, the design procedure and simulated and measured results will be presented. The conversion efficiency and noise figure are found to be suitable for a short range. Phase noise at IF is low.

II. Mixer Configuration

In this section, the design for a receiver operating at the 61–62-GHz band with an internally generated 30-GHz LO is presented. In Section II-A, a description of the circuit is given and design philosophy is discussed. The quasi-Yagi antenna's characteristics essential for this circuit is discussed in Section II-B.

A. Mixer Layout

Fig. 1 shows a photograph and circuit architecture of the prototype second harmonic SOM. The architecture consists of a balanced SOM circuit integrated with a broad-band quasi-Yagi antenna with a balanced microstrip feed. The 30-GHz DR push–pull oscillator operates as a balanced second harmonic gate mixer and generates the internal LO. The push–pull operation causes the internally generated waveforms of each device to be in antiphase at the fundamental frequency and in phase at the second harmonic. The RF signal received at the antenna feeds will be in antiphase due to balanced nature of the antenna feed. When the broad-band antenna is connected to the balanced SOM, broad-band antiphase excitation of the SOM is achieved, and the need of a balun is avoided. IF signals are then extracted from the drain currents with a bandstop filter (fundamental and second harmonic frequencies). The channels are combined out of phase with an external hybrid for signal detection. LO filtering is placed at the antenna feed to suppress LO leakage. Additionally, since the second harmonic is in phase, automatic suppression of second harmonic radiation is achieved due to the balanced nature of the antenna.

The use of a second harmonic SOM allows the use of lower $f_{\max}$ devices, which should typically reduce system cost. In this case, general-purpose low noise K-band pseudomorphic high electron-mobility transistors (pHEMTs) with $0.25 \times 200\ \mu\mathrm{m}^2$ gate were used for the SOM (Fujitsu model FHR02X). The devices are connected with 0.7-mil bondwire to a 5-mil alumina substrate.

A DR ($\varepsilon_r = 30$, $Q_0 = 12000$ at 10 GHz) with a diameter and a thickness of 89 and 27 mil is placed on a 25-mil quartz cube in an open cylindrical copper cavity to couple the gates at 30 GHz. The cavity diameter was 173 mil and the height was 120 mil. This structure is mounted on the alumina circuit board to form the resonator of the SOM. The loaded Q of the resonator is 900 at the fundamental. Simulation did not show any spurious resonance within the 58–62-GHz band. At the fundamental, the resonator was modeled as a parallel *RLC* network coupled with two transformers to the microstrip lines. The element values in the *RLC* network were defined by the measured fundamental resonance frequency and unloaded Q, and the measured loaded Q defined the transformer ratios.

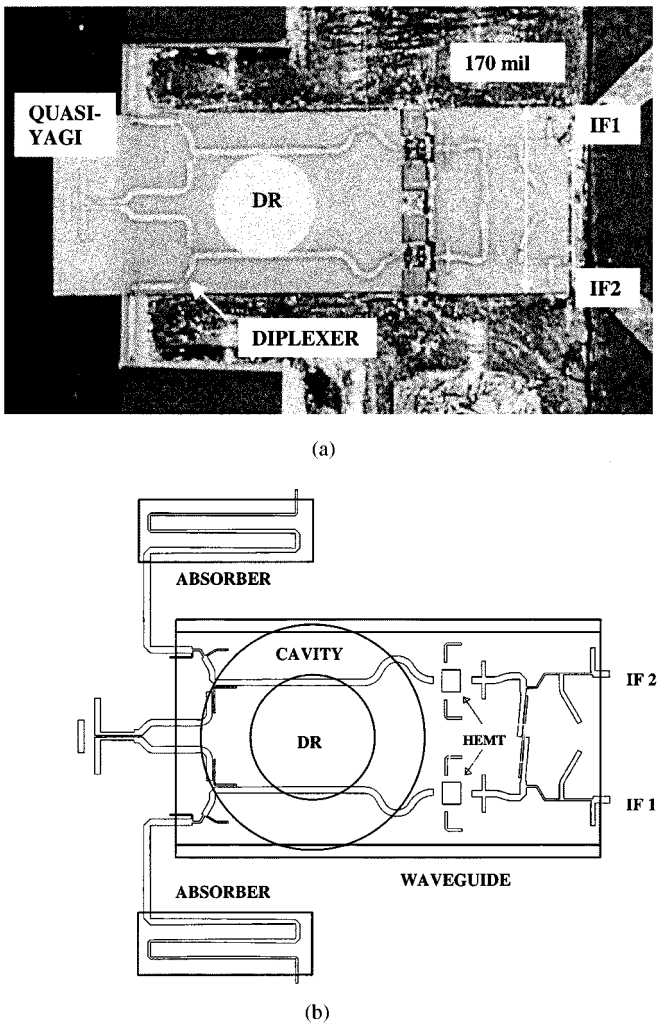

Fig. 1. (a) Photograph and (b) schematic of the 60-GHz SOM with an integrated quasi-Yagi antenna on 5–mil alumina substrate.

Proper design of the impedance seen by the gate and drain is essential for optimum performance. For the resonator circuit to function properly at the fundamental frequency, the gate side of the device must be terminated with 50 Ω. This is achieved by the 50-Ω line terminated with an absorber, as shown at the top and bottom left-hand side of Fig. 1(b). Weak DR coupling is then adopted at the gate. A low-pass filter is used to suppress RF leakage at these lossy terminations. Additionally, diplexers separate the resistive terminations from the antenna, thus eliminating odd-mode fundamental frequency coupling through the antenna feed network at the gain bandwidth (0–35 GHz), as well as reducing any radiation from the antenna. A coupled-line coupler is used to share the fundamental frequency drain currents. Due to symmetry, a virtual short exists at the center of the filter at the fundamental frequency. Thus, the drain of each device will see a reactive load. Additionally, source stubs are needed to enhance the instability at the fundamental frequency to satisfy the oscillation condition. Brass posts, which were connected with conducting epoxy, shorted the source stubs.

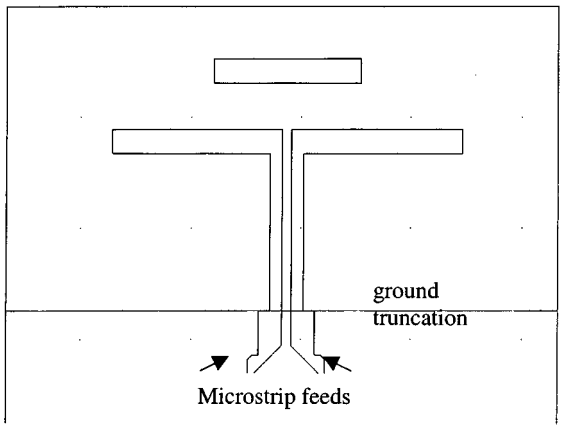

Fig. 2. Quasi-Yagi antenna with dual feed.

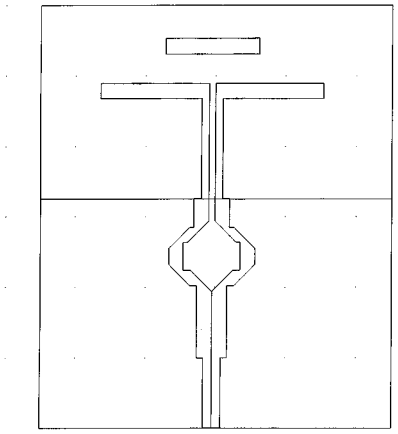

Fig. 3. Test structure for even-mode excitation.

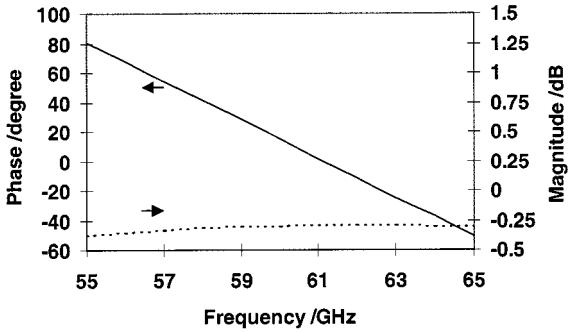

Fig. 4. Simulated return loss of the test structure in Fig. 3.

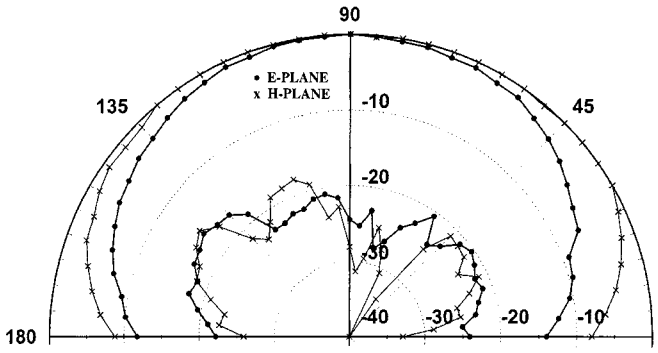

Fig. 5. Measured quasi-Yagi antenna patterns at 60 GHz.

To simplify the design, both gate and drain should have a reactive load at the second harmonic frequency. The sensitivity against parametric variations of the coupler are reduced by doing the required second harmonic impedance for optimal mixing performance with stub pair matching networks.

The endfire quasi-Yagi antenna is placed in direct proximity of the DR cavity, reducing RF losses and minimizing circuit size. This is possible because the backside radiation of the endfire antenna is low. The DR cavity does not, therefore, affect the radiation characteristics of the antenna. Additionally, the circuit is placed in waveguide with a cutoff frequency of 30.6 GHz, reducing fundamental frequency radiation. The waveguide and resonator cavity were milled from the same block as shown in Fig. 1(b). The gate and drain bias circuits were made on 31 mil ($\varepsilon r = 2.33$) RT/Duroid. Drain bias was fed through a 20-nH inductor and 100-Ω resistor. Gate bias was fed through a 50-kΩ resistor. The mixer/antenna circuit and bias circuits were assembled on a brass carrier. The alumina substrate with the mixer and antenna are mounted so that no brass is under the antenna. This is essential for proper radiation of the quasi-Yagi antenna, which relies on truncation of the microstrip ground plane. The edge of the brass carrier is covered with an absorber along the antenna side, giving 8-dB return loss at RF. This reduces scattering from the carrier.

B. Quasi-Yagi Antenna

A 60-GHz dual-feed quasi-Yagi antenna on 5-mil alumina, as shown in Fig. 2, was used for reception. With odd-mode excitation, the antenna radiates. The odd-mode input impedance of each microstrip feed is 50 Ω. At even-mode excitation, radiation is suppressed due to the truncated ground plane at the transition from coupled microstrip-to-coplanar stripline, which does not support an even mode.

Therefore, the impedance looking toward the antenna at the truncation can be modeled as capacitance when even-mode excitation is applied. This even-mode capacitance was defined with the test structure shown in Fig. 3. The return loss of the structure was simulated with an EM simulator (HP HFFS), with the response shown in Fig. 4. Next, the structure was simulated with only the microstrip portion in a circuit simulator (HP Series IV) with each coupled microstrip feed terminated in a capacitor to ground. The proper capacitance was obtained by optimizing the value until the phase response of the equivalent circuit fit the phase response of the full-wave simulation of the entire structure. An overall error less than 2° over the entire simulated frequency range was obtained with a capacitance value of 93 fF terminating each feed arm. From the circuit simulation of the microstrip feed, 0.2 dB of the return loss shown in Fig. 4 was identified to be due to metal and dielectric losses and, hence, the radiation resistance for even-mode excitation was omitted. Simulated gain for an antenna with a single balun feed was 5.9 dB in the frequency range from 58 to 62 GHz, and was used later to characterize the dual-feed antenna. For the noise simulation, the s-parameters of the antenna as a two-port structure were simulated. In this case, a simple equivalent circuit is not sufficient and the data were used directly. The measured patterns are shown in Fig. 5.

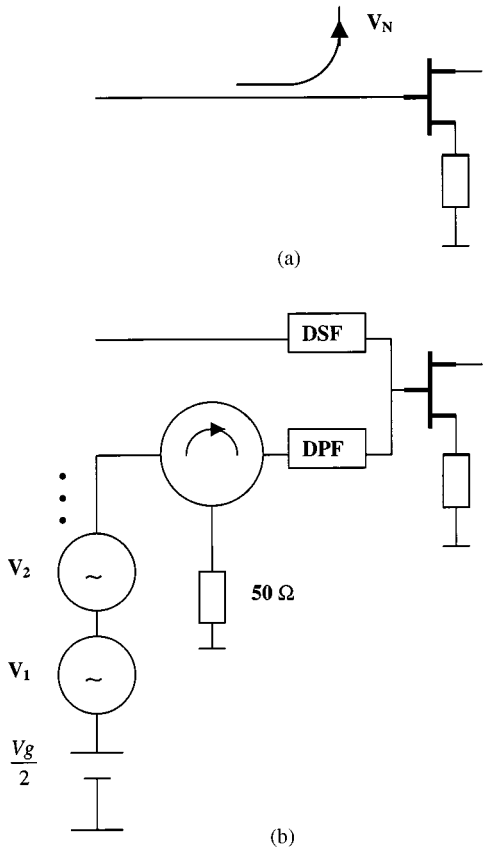

Fig. 6. (a) Oscillator harmonics extracted in the oscillator simulation are used in (b) a regular mixer simulation.

III. Nonlinear Simulations of Integrated-Antenna SOM

Accurate analysis of SOM circuits is not a trivial task. As shown in [12], time-domain analysis with high Q circuits requires a large amount of time steps and achieving convergence can be difficult. Additionally, existing circuit simulators cannot directly perform a harmonic-balance simulation of SOM circuits. However, by successively analyzing the structure as an oscillator and mixer, meaningful results can be obtained if the RF power is low. For these reasons, harmonic balance techniques were preferred as a straightforward alternative to transient analysis. A commercially available black-box large-signal model for the device was used in the simulation. First, the oscillator analysis is used to extract the large-signal voltage waveform at the gate of the FET, as shown if Fig. 6(a). For this analysis, the amplitude and phase for the first three harmonics were used. This oscillation waveform is then incorporated into the mixer simulation by applying it to the gate of the device, as shown in Fig. 6(b). The delta pass filter (DPF) is used to couple only the dc and oscillation frequency harmonics. The delta stop filter (DSP) injects the RF signal, thus separating the oscillation and RF signals.

In the oscillator simulation, the goal was to maximize the second harmonic current in the channel. The device was biased close to cutoff, where second harmonic generation is effective and no excess noise is generated. Additionally, source, drain, and gate impedances calculated by using the symmetry of the circuit and known excitation were optimized. At the fundamental frequency, it was found that the source has high impedance, while the drain has low impedance. The second harmonic source impedance is slightly capacitive and the drain impedance highly inductive.

Fig. 7(a) shows the simulated conversion efficiency, return loss, and second harmonic source and drain node current variations when source stub is varied from 0.125 to 0.25 of the fundamental wavelength (L_1) and the drain stub had the optimum value obtained from the oscillator simulation. From this, we see that a short source stub does not give enough gain to generate the necessary harmonics. With long source stubs, the conversion efficiency drops gradually as input mismatch increases. Therefore, an optimum value of 0.175 L_1 is chosen where both currents are close to the local current maximum.

Fig. 7(b) shows results when the drain stub length is varied, while source stub length has the optimum value obtained previously. Moving the resonator eliminated load pulling. It was found that the drain stub length affects primarily the second harmonic impedance, while the fundamental frequency reactance varies smoothly from $j15$ to $j35$ in the simulated range. Although the source current has a maximum at 0.18 L_1, due to very high drain impedance, and the drain current has a maximum at 0.20 L_1 due to zero impedance, neither of these lengths do not optimize conversion efficiency. Instead, the optimum value was chosen to be 0.08 L_1, where conversion frequency sensitivity is not high, and fundamental current is minimally affected. Note that, for a 60-GHz RF signal, the optimum source and drain stub lengths are predicted by the respective currents of the first current maximum in Fig. 5(a) and (b).

The internally generated even-mode excitation (second harmonic) is phased to add up at the device gate. The effect of the phasing angle is shown in Fig. 7(c) by varying the distance between the antenna feed and diplexer from 0° to 180° and by using the optimum values of Table I at source and drain. The effect of phasing is embedded in LO. Conversion efficiency and return loss are shown as a function of phasing angle. From this, we see that phasing angle and RF minimally affects them. The operation point was chosen at 93°, where gate load is inductive.

The optimum node impedances of Fig. 8 are shown in Table I. Bond-wire effects were included in the calculation. The drain to source impedances at LO harmonics result to zero in optimum gate mixer with an external LO [12]. In the SOM, case zero impedance is not possible at the fundamental frequency because a vertical load line does not provide feedback. A high impedance was needed here to boost the gate swing due to the harmonic nature of operation and a bias above pinchoff voltage. After adding the device parasitics the sum of Z_1 and Z_2 is less than 1/4 of Z_3. The second harmonic impedance is not critical for conversion efficiency, as seen in Fig. 7(c), but affects the phase noise by modifying the load cycle [13].

In the noise simulation, the s-parameters of the antenna as a two-port are effective for uncorrelated noise sources. Noise temperature at the output was found to be about 1700 K, and DSB noise figure is thus about 7 dB higher than conversion loss.

IV. Experimental Results

The RF to IF conversion efficiency was measured by illuminating the receiver from the endfire direction with a horn antenna, and combining the IF channels with an external hybrid.

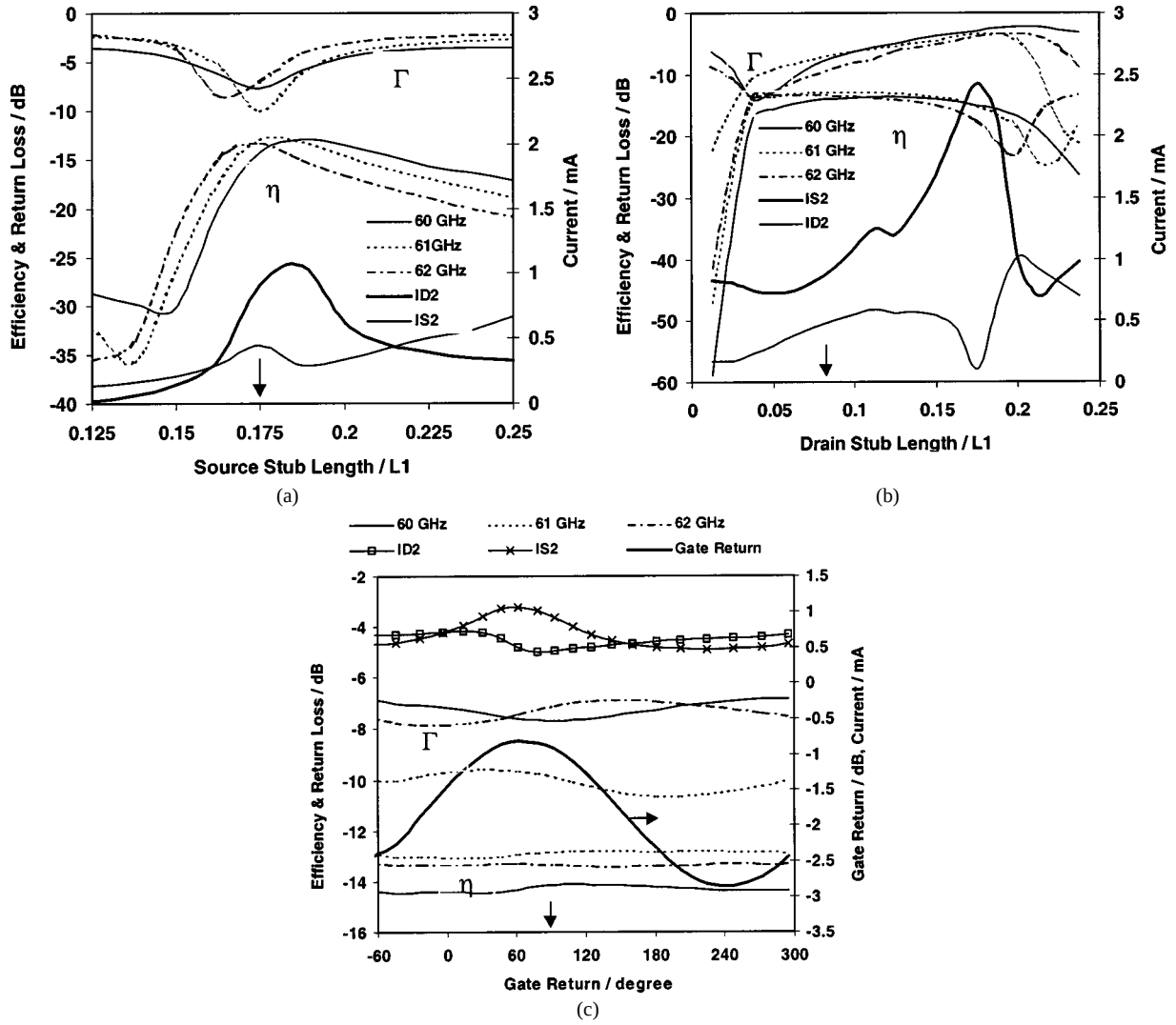

Fig. 7. Simulated return loss (Γ), conversion efficiency (η), second harmonic drain (ID2), and source (IS2) node current as a function of source stub length, drain stub length, and gate return phase in (a)–(c), respectively. Drain bias was 1.5 V and gate bias was −0.6 V.

Conversion efficiency was calculated by relating the measured IF power to calculated available RF power at the receiver antenna port and calculating the isotropic conversion loss [14]. Available RF power was calculated by using the Friis transmission formula with known antenna separation, horn antenna gain and input power, and simulated quasi-Yagi antenna gain. The RF signal was generated with a synthesized sweeper (HP 8340A), an amplifier (HP 8349B), and a pentupler (HP 85 100V) with an isolator at the output. A Klystron was used when more than 0 dBm power was needed. Power was calibrated at the isolator output at each frequency point with a power meter (ML83A) and power head (MP716A). IF power was measured with a spectrum analyzer (HP 8562A).

The measured and calculated RF to IF conversion efficiency over a 4-GHz bandwidth with a fixed −40-dBm input power is shown in Fig. 9. From this, we see that a conversion loss of 15 dB was achieved over a 1.5-GHz bandwidth. When the channels were combined in phase, the level was reduced by 15 dB, showing that the circuit is functioning effectively as a balanced receiver. Reduced conversion efficiency at the lower frequencies is accounted for by RF mismatch. Simulated return loss is shown in Fig. 10. At the low-frequency end, the matching is poor.

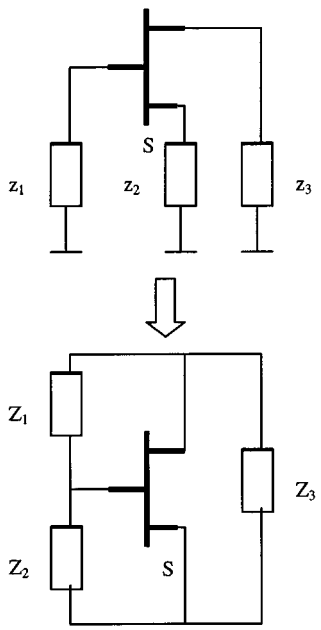

Fig. 8. Transformation of the device load impedances.

TABLE I
IMPEDANCES FOR OPTIMUM CONVERSION EFFICIENCY

Harmonic	z_1 /Ω	z_2 /Ω	z_3 /Ω	Z_1 /Ω	Z_2 /Ω	Z_3 /Ω
1	7+j 27	+j84	+j18	9+j52	37+j216	14+ j 152
2	5+j47	-j25	+j57	+j1.3	+j2.2	+j 1.8

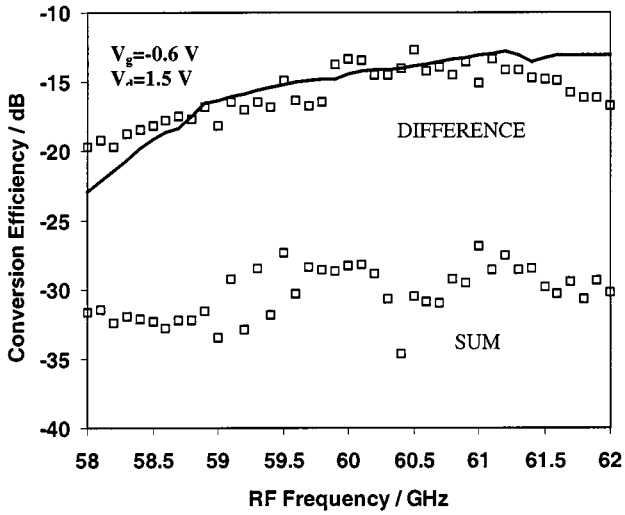

Fig. 9. Simulated (solid line) and measured conversion efficiency as function of RF frequency. The measured response by summing the channels is also shown.

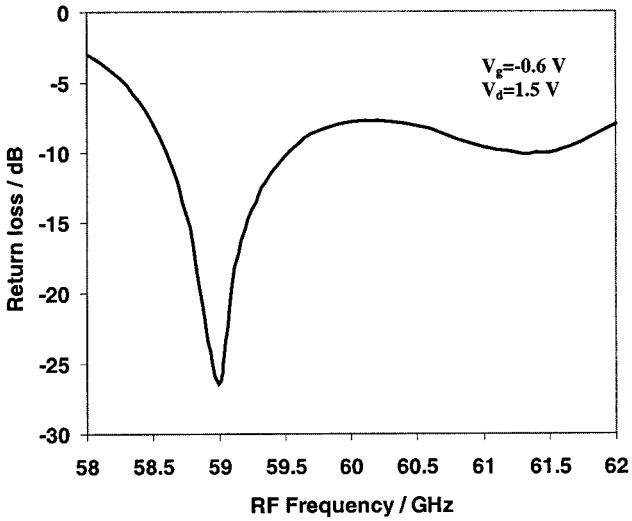

Fig. 10. Simulated return loss.

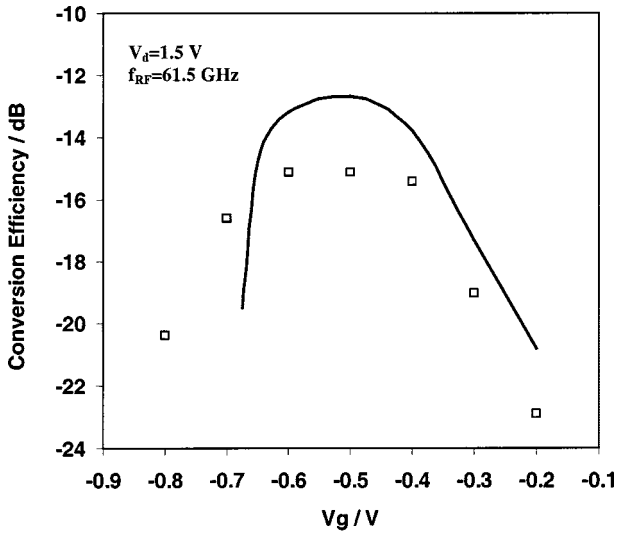

(a)

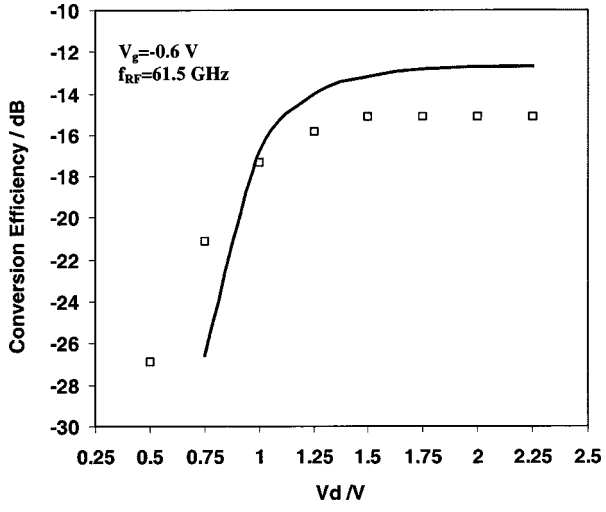

(b)

Fig. 11. Simulated (solid line) and measured conversion efficiency as a function of gate and drain bias in (a) and (b), respectively.

The sensitivity of the conversion loss to gate and drain bias voltage is shown in Fig. 11(a) and (b), respectively. From this, the 1-dB gate voltage window is 0.3 V centered at −0.5 V, and the conversion loss saturates with 1.5 V applied to the drain (11 mA).

Next, the conversion efficiency as a function of RF input power with a fixed operating frequency of 61.5 GHz was measured by placing the antenna at a rectangular waveguide opening (WR-15) and by measuring the IF power as a function of RF power available to mixer. The power was calibrated by using the measured conversion loss. Fig. 12 shows the result of the measurement. Deviation from linear response is 1 dB at 3-dBm RF input. The second IF ($4 f_{\mathrm{OSC}} - 2 f_{\mathrm{RF}}$) was also measured. Fig. 13 shows the simulated single-channel level of the second IF and the measured combined result. Ideally, the measured response should be zero for an even-order product combined out of phase. Here, the cancellation goes slightly below the simulated single-channel response. Measured level is about 60 dB below the first IF.

Fundamental frequency and second harmonic radiation leakage from the circuit was also determined by measuring radiation at the endfire beam direction. Radiated power was measured by using harmonic mixers (HP 11970A and

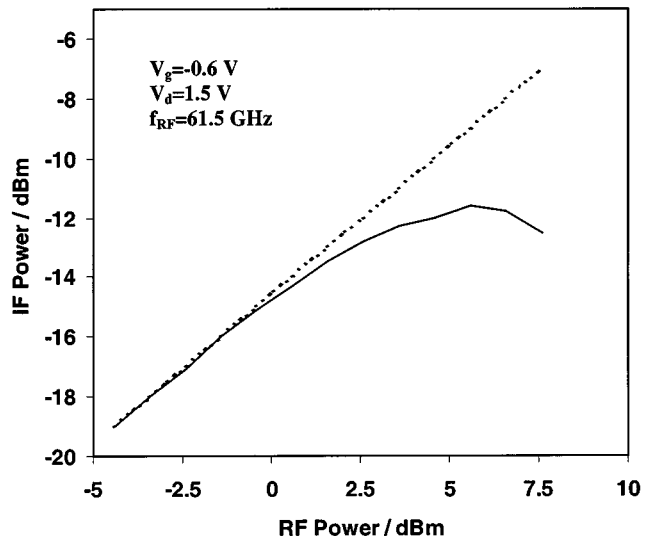

Fig. 12. IF power measured as a function of RF power (dashed line simulates linear response).

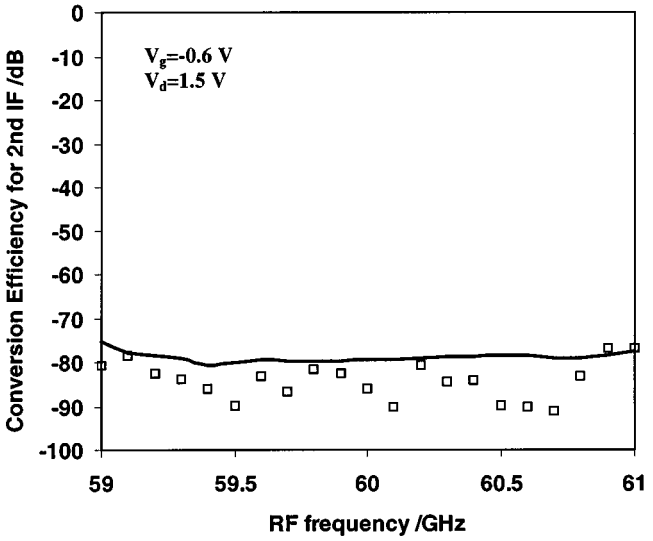

Fig. 13. Simulated (line) single channel and measured conversion efficiency for the second IF.

11970V). Second harmonic radiation was −26 dBm (by assuming odd-mode excitation).

The IF phase noise was −95 dBc/Hz at 100 kHz, as extracted from Fig. 14. For a 60-GHz free-running HEMT source this is a reasonably low value. Fig. 15 shows the measured and simulated DSB noise figure as a function of RF frequency. Measured IF output noise was −170 dBm/Hz at frequencies higher than 50 MHz, giving an DSB noise figure 4 dB higher than conversion loss. The receiver-input sensitivity is thus −155 dBm/Hz in the previous frequency range.

One possible disadvantage of an SOM receiver is the possibility that the oscillator will injection lock to the RF signal. To first order, this balanced oscillator should not lock to incoming RF because the generated locking signals ($f_{\mathrm{RF}} - f_{\mathrm{OSC}}$) will be in even mode, which is not supported by push–pull configuration. However, in practice, as shown in Fig. 16, the overharmonic locking bandwidth as a function of

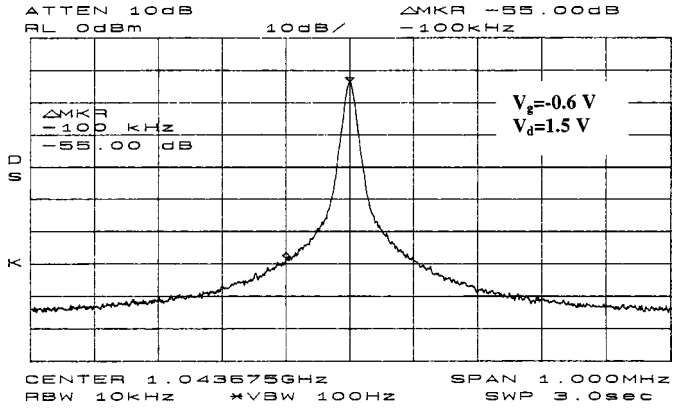

Fig. 14. Spectrum of the IF signal.

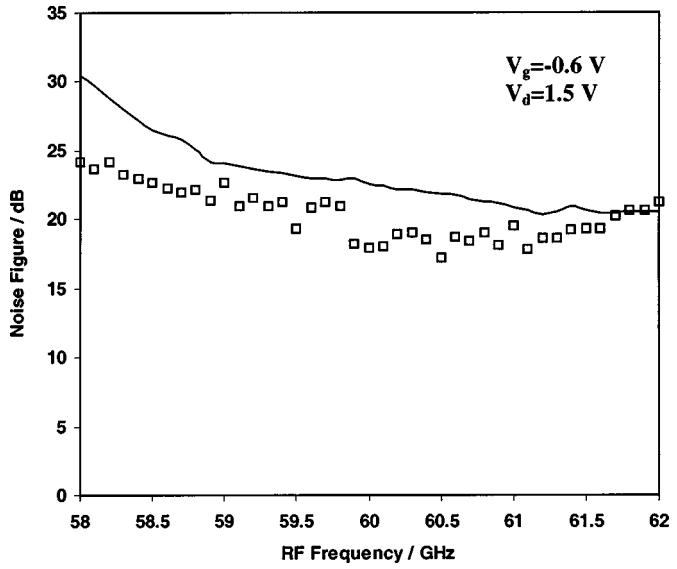

Fig. 15. Simulated (line) and measured DSB noise figure.

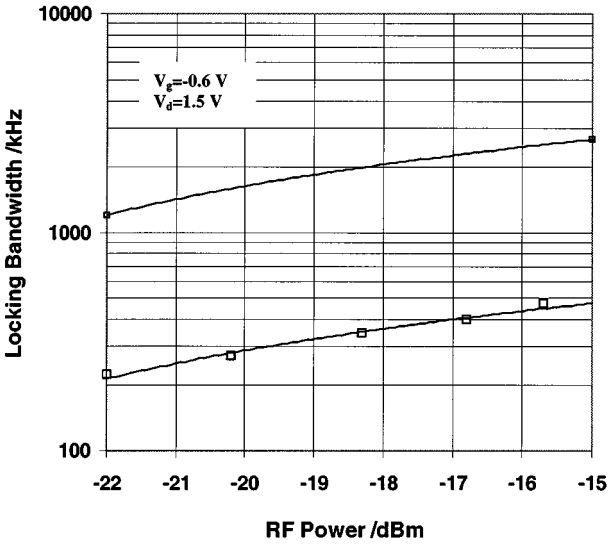

Fig. 16. Simulated (line) and measured injection-locking bandwidth as a function of RF power in the case of 15-dB imbalance between the channels. The upper curve assumes a pure even-mode RF excitation.

RF power can be measured (the measurement setup for Fig. 12 was also used here). We see that the measured points closely

follow the curve of the formula for subharmonic injection locking $\Delta f_1 = (f_{\rm OSC}/2Q_L)\sqrt{(P_{1/2}/P_0)}$ [15], where the rational index was changed to an integer and vice versa. The effective even-mode part of the RF was calculated by using the measured unbalance 15 dB of Fig. 9 at 60 GHz, in this way, an odd-mode locking signals are available for the formula. Also, the simulated locking bandwidth with purely even-mode RF excitation is shown in Fig. 16, and the measured locking bandwidth is 20% of this. The mixing products are linearly related to RF power at these power levels. The required locking power is quite high, thus, injection locking is highly unlikely.

V. Discussion and Conclusions

A balanced second harmonic antenna integrated SOM at 60 GHz has been demonstrated in this paper. The antenna was used as a mode filter, operating as a 180° balun for RF, and reflecting back the internally generated second harmonic. The second harmonic radiation was reduced by more than 20 dB compared to the power that is available at the gate side. The measured and simulated conversion efficiency correlate and the highest conversion efficiency are comparable with the results obtained in [4], [6]. The measured bandwidth was limited by the diplexer because the antenna operates up to 70 GHz. The optimization of a Doppler SOM and SOM with an IF at 1 GHz was found to be different. The observed conversion efficiency saturation suggests that an optimum design is achievable in terms of device gain and circulating fundamental power, which will minimize dc power consumption. With typical reception levels, neither conversion efficiency degradation nor injection locking is a problem. Therefore, the transmitter and receiver can be placed just centimeters apart if necessary. Observed locking bandwidth was found to be due to imbalance in RF coupling and conversion.

A DR was used to stabilize the frequency, and the obtained IF phase noise is comparable to [16]. In [17], a cavity-stabilized Gunn oscillator was used as an external LO in a receiver, and the 50-Mb/s data on 60-GHz carrier data was recovered. Thus, a typical millimeter-wave local area network (LAN) receiver architecture [17], [18] could be simplified with a subharmonic SOM in some applications.

Acknowledgment

The authors would like to thank the Center for High Frequency Electronics, University of California at Los Angeles (UCLA), for the computing, measuring, and dicing capabilities. The authors also wish to express their appreciation to Dr. W. R. Deal, Malibu Networks, Los Angeles, CA, for his hours of editing this paper's manuscript.

References

[1] Y. Qian, W. R. Deal, N. Kaneda, and T. Itoh, "Microstrip fed quasi-Yagi antenna with broadband characteristics," *Electron. Lett.*, vol. 34, no. 23, pp. 2194–2196, Nov. 1998.

[2] I. D. Higgins, "Performance of self-oscillating GaAs MESFET mixer at X-band," *Electron. Lett.*, vol. 12, no. 23, pp. 605–606, Nov. 11, 1976.

[3] Y. Tajima, "GaAs FET applications for injection-locked oscillators and self-oscillating mixers," *IEEE Trans. Microwave Theory Tech.*, vol. MTT-27, pp. 629–632, July 1979.

[4] D. H. Evans, "A millimeter-wave self-oscillating mixer using a GaAs FET harmonic-mode oscillator," in *IEEE MTT-S Int. Microwave Symp. Dig.*, 1986, pp. 601–604.

[5] V. D. Hwang and T. Itoh, "Quasioptical HEMT and MESFET self-oscillating mixers," *IEEE Trans. Microwave Theory Tech.*, vol. 36, pp. 1701–1705, Dec. 1988.

[6] M. J. Roberts, S. Iezekiel, and C. M. Snowden, "A compact subharmonically pumped MMIC self oscillating mixer for 77 GHz applications," in *IEEE MTT-S Int. Microwave Symp. Dig.*, 1998, pp. 2104–2108.

[7] M. J. Roberts, N. Bourhill, S. Iezekiel, D. P. Steenson, and C. M. Snowden, "Opto electronic mixing in MMIC W-band self-oscillating mixer," *Electron. Lett.*, vol. 34, no. 9, pp. 904–905, 1998.

[8] H. Sawada and N. Imai, "A self-oscillating up-converter using a heterojunction bipolar transistor up to millimeter-wave bands," in *Proc. Int. Topical Microwave Photon. Meeting*, 1996, pp. 153–156.

[9] L. Dussopt and J.-M. Laheurte, "Cavity backed antenna integrating a self-oscillating mixer," *Microwave Opt. Technol. Lett.*, vol. 21, no. 2, pp. 156–158, Apr. 1999.

[10] X. Zhou, X. Zhang, and A. S. Daryoush, "A phase controlled self-oscillating mixer," in *IEEE MTT-S Int. Microwave Symp. Dig.*, 1994, pp. 749–752.

[11] I. Kipnis and A. P. Khanna, "Large-signal computer-aided analysis and design of silicon bipolar MMIC oscillators and self-oscillating mixers," *IEEE Trans. Microwave Theory Tech.*, vol. 37, pp. 558–564, Mar. 1989.

[12] S. A. Maas, "Design and performance of a 45-GHz HEMT mixer," *IEEE Trans. Microwave Theory Tech.*, vol. MTT-34, pp. 799–803, July 1986.

[13] P. Andre, J. M. Dienot, O. Llopis, R. Plana, M. Gayral, and J. Grffeuil, "Microwave oscillator design from load cycle optimization, application to MMIC GaAs MESFET oscillator," in *Proc. 24th European Microwave Conf.*, vol. 1, 1994, pp. 831–835.

[14] K. D. Stephan and T. Itoh, "A planar quasioptical subharmonically pumped mixer characterized by isotropic conversion loss," *IEEE Trans. Microwave Theory Tech.*, vol. MTT-32, pp. 97–102, Jan. 1984.

[15] X. Zhang, X. Zhou, B. Aliener, and A. S. Daryoush, "A study of a subharmonic injection locking for local oscillator," *IEEE Microwave Guided Wave Lett.*, vol. 2, pp. 97–99, Mar. 1992.

[16] K. M. Funabashi, T. Inoue, K. Ohota, K. Maruhashi, K. Hosoya, M. Kuzuhara, K. Kanekawa, and Y. Kobayashi, "A 60-GHz MMIC stabilized frequency source composed of a 30 GHz DRO and a doubler," in *IEEE MTT-S Int. Microwave Symp. Dig.*, 1995, pp. 71–73.

[17] K. Kojucharow, H. Kaluzni, M. Sauer, and W. Nowak, "A wireless LAN at 60 GHz—Novel system design and transmission experiments," in *MTT-S Int. Microwave Symp. Dig.*, 1998, pp. 1513–1516.

[18] T. Ninomiya, T. Saito, Y. Ohashi, and H. Yatsuka, "60-GHz transceiver for high-speed wireless LAN system," in *MTT-S Int. Microwave Symp. Dig.*, 1996, pp. 1171–1174.

Mikko Sironen, photograph and biography not available at time of publication.

Yongxi Qian (S'91–M'93) was born in Shanghai, China, in 1965. He received the B.E. degree from Tsinghua University, Beijing, China, in 1987, and the M.E. and Ph.D. degrees from the University of Electro-Communications, Tokyo, Japan, in 1990 and 1993, respectively, all in electrical engineering.

From 1993 to 1996, he was an Assistant Professor at the University of Electro-Communications. In April 1996, he joined the University of California at Los Angeles (UCLA), where he is currently an Assistant Research Engineer in the Electrical Engineering Department. He has performed research on various numerical techniques for microwave and millimeter-wave circuits and antennas, generation and transmission of picosecond electrical pulses, crosstalk problems in high-density MMICs, miniature circuits for mobile communications, and a 60-GHz millimeter-wave focal plane imaging array. He has authored or co-authored over 160 refereed journal and conference papers, two books, and several book chapters. His current research interests include broad-band planar antennas, smart antennas and arrays for wireless communications, high-efficiency microwave power amplifiers, RF interconnect for mixed-signal silicon MMICs, quasi-optical power-combining photonic bandgap (PBG) structures, active integrated antennas for indoor LANs, and high-power broad-band RF photonic devices for millimeter- and submillimeter-wave photomixing.

Dr. Qian was the recipient of the Japan Microwave Prize presented at the 1998 Asia–Pacific Microwave Conference and Best Student Paper Award (as co-author) presented at the 1999 29th European Microwave Conference.

Tatsuo Itoh (S'69–M'69–SM'74–LM'82) received the Ph.D. degree in electrical engineering from the University of Illinois at Urbana-Champaign, in 1969.

From September 1966 to April 1976, he was with the Electrical Engineering Department, University of Illinois at Urbana-Champaign. From April 1976 to August 1977, he was a Senior Research Engineer in the Radio Physics Laboratory, SRI International, Menlo Park, CA. From August 1977 to June 1978, he was an Associate Professor at the University of Kentucky, Lexington. In July 1978, he joined the faculty at The University of Texas at Austin, where he became a Professor of electrical engineering in 1981 and Director of the Electrical Engineering Research Laboratory in 1984. During the summer of 1979, he was a Guest Researcher at AEG-Telefunken, Ulm, Germany. In September 1983, he was selected to hold the Hayden Head Centennial Professorship of Engineering at The University of Texas at Austin. In September 1984, he was appointed Associate Chairman for Research and Planning of the Electrical and Computer Engineering Department, The University of Texas at Austin. In January 1991, he joined the University of California at Los Angeles, as Professor of electrical engineering and Holder of the TRW Endowed Chair in Microwave and Millimeter Wave Electronics. He was an Honorary Visiting Professor at the Nanjing Institute of Technology, Nanjing, China, and at the Japan Defense Academy. In April 1994, he became an Adjunct Research Officer for Communications Research Laboratory, Ministry of Post and Telecommunication, Japan. He currently holds a Visiting Professorship at The University of Leeds, Leeds, U.K., and is an External Examiner of the Graduate Program of City University of Hong Kong. He has authored or co–authored 265 journal publications, 515 refereed conference presentations, and 30 books/book chapters in the area of microwaves, millimeter-waves, antennas and numerical electromagnetics. He has also generated 43 Ph.D. students.

Dr. Itoh is a member of the Institute of Electronics and Communication Engineers of Japan, and Commissions B and D of USNC/URSI. He served as Editor-in-Chief of the IEEE TRANSACTIONS ON MICROWAVE THEORY AND TECHNIQUES (1983–1985). He serves on the Administrative Committee of the IEEE Microwave Theory and Techniques Society (IEEE MTT-S). He was Vice President of the IEEE MTT-S in 1989 and President in 1990. He was Editor-in-Chief of IEEE MICROWAVE AND GUIDED WAVE LETTERS (1991–1994). He was elected as an Honorary Life Member of the IEEE MTT-S in 1994. He was the chairman of USNC/URSI Commission D (1988–1990), and chairman of Commission D of the International URSI (1993–1996). He is chair of the Long-Range Planning Committee of URSI. He serves on advisory boards and committees of a number of organizations. He has been the recipient of a number of awards, including the 1998 Shida Award presented by the Japanese Ministry of Post and Telecommunications and the 1998 Japan Microwave Prize.